

Nucleation of reversed domains at grain boundaries

T. Schrefl

Institute of Applied and Technical Physics, T. U. Vienna, Wiedner Hauptstrasse 8, A-1040 Vienna, Austria, and Max-Planck-Institut für Metallforschung, Institut für Physik, Heisenbergstrasse 1, 7000 Stuttgart 80, Germany

H. F. Schmidts

Max-Planck-Institut für Metallforschung, Institut für Physik, Heisenbergstrasse 1, 7000 Stuttgart 80, Germany

J. Fidler

Institute of Applied and Technical Physics, T. U. Vienna, Wiedner Hauptstrasse 8, A-1040 Vienna, Austria

H. Kronmüller

Max-Planck-Institut für Metallforschung, Institut für Physik, Heisenbergstrasse 1, 7000 Stuttgart 80, Germany

Micromagnetic analysis using a finite-element technique confirms that intergrain magnetostatic and exchange interactions drastically affect the magnetization reversal mechanism in nucleation controlled permanent magnets. The investigation of the nucleation fields of magnetically coupled grains emphasizes the important role of nonmagnetic boundary phases and well-aligned grains for the enhancement of coercivity. The long-range magnetostatic interactions between the grains reduce the coercive field of ideally oriented particles. The exchange coupling of misoriented neighboring grains causes a strongly inhomogeneous magnetic state near the interface of the particles which favors the nucleation of reversed domains. Intergrain exchange interactions considerably reduce the coercive field, especially if the angle between the easy axes of adjacent grains is high. An algorithm for adaptive mesh refinement controls the discretization error throughout the calculation of the demagnetization curves.

I. INTRODUCTION

The coercivity of technical permanent magnets approaches only 20%–40% of the theoretical nucleation fields derived from micromagnetic theory as developed by Brown¹ and Stoner and Wohlfarth.² The discrepancy between the experimental and the theoretical values for the nucleation field is generally attributed to the microstructure of permanent magnets.³

Previous articles^{4,5} dealing with the nucleation of reversed domains show that magnetic inhomogeneities reduce the coercivity of Nd₂Fe₁₄B magnets considerably. Recently intergrain interactions were found to be an additional factor reducing the nucleation field. Fukunaga and Inoue⁶ investigated intergrain exchange and magnetostatic interactions in isotropic Nd₂Fe₁₄B magnets. The exchange interaction between the grains reduces the coercive field considerably if the grain size is sufficiently small (≤ 50 nm). Hernando, Navarro, and González⁷ presented a one-dimensional micromagnetic model for the investigation of intergrain exchange coupling. The formation of a domain-wall-like magnetization distribution at the interfaces of exchange coupled grains leads to a significant reduction of the nucleation field.

In this study the interactions of two hard magnetic grains of hexagonal cross section have been numerically investigated using a finite-element technique. The surfaces of the grains have been assumed to be magnetically perfect without any inhomogeneities. The demagnetization curves of interacting grains with various degrees of alignment have been calculated for Nd₂Fe₁₄B and SmCo₅ magnets.

II. SIMULATION MODEL

The minimization of the total Gibbs free energy with respect to the spontaneous magnetic polarization \mathbf{J}_s , subject to the constraint $|\mathbf{J}_s| = J_s$, provides a stable equilibrium state of a magnetic structure. The total magnetic free enthalpy ϕ_G can be written in the form

$$\begin{aligned} \phi_G[\mathbf{J}_s(\mathbf{r})] = & \int \int dV [K_1 \sin^2 \varphi(\mathbf{r}) + K_2 \sin^4 \varphi(\mathbf{r}) \\ & + A[\nabla_r \varphi(\mathbf{r})]^2 - \mathbf{h}_{\text{ext}} \cdot \mathbf{J}_s(\mathbf{r}) \\ & - (\tfrac{1}{2}) \mathbf{H}_d(\mathbf{r}) \cdot \mathbf{J}_s(\mathbf{r})], \end{aligned} \quad (1)$$

where K_1 , K_2 are the anisotropy constants, A is the exchange constant, φ is the angle of the spontaneous magnetic polarization \mathbf{J}_s with respect to the easy axis, and \mathbf{h}_{ext} is the external field. The requirement that the first variation vanishes leads to the two-dimensional micromagnetic equation for uniaxial magnetic particles.⁸ The demagnetizing field \mathbf{H}_d , whose source is \mathbf{J}_s , couples the micromagnetic equation with Poisson's equation for the magnetic scalar potential. An iterative numerical algorithm determines the equilibrium states: Starting with the saturated state (i) the demagnetizing field of the distribution of the spontaneous magnetic polarization follows from the solution of Poisson's equation, (ii) using this demagnetizing field the micromagnetic equation is solved to obtain a new polarization distribution. This algorithm is repeated until a self-consistent set of \mathbf{H}_d and \mathbf{J}_s vectors on the finite-element

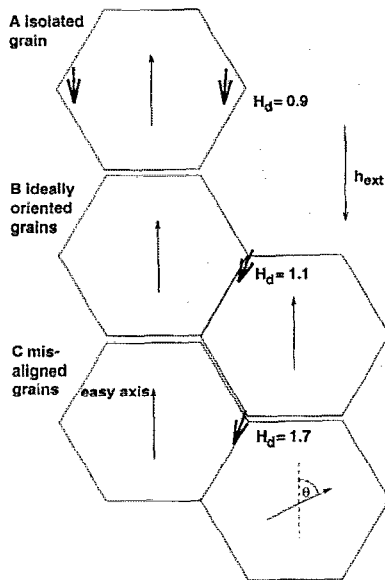


FIG. 1. Particle configurations used for the simulations. The bold arrows indicate the direction of the demagnetizing field H_d in the critical regions where the absolute value of H_d reaches its maximum. The absolute value of the demagnetizing field for zero applied field is given in units of J/μ_0 .

mesh is obtained. The repeated calculation of the equilibrium state for decreasing external field provides the demagnetization curve of the magnetic particles.

In numerical micromagnetic calculations the inhomogeneous equilibrium states of the spontaneous magnetic polarization J_s and the demagnetizing field H_d lead to significant discretization errors.⁹ Since the magnetization states vary during the calculation of the demagnetization curve, a refinement scheme has to adapt the finite-element mesh according to the requirements of the current magnetization state. A refinement technique used in a general purpose electric or magnetic analysis code¹⁰ has been extended to micromagnetic applications.¹¹ Convergence tests showed that the nucleation field can be calculated with a relative accuracy of about 5%.

III. PARTICLE CONFIGURATIONS

The particle systems used for the simulation are shown in Fig. 1. The particles of $5\ \mu\text{m}$ diameter have hexagonal cross section. The isolated grain of case A provides reference calculations. The ideally oriented particles of case B and the misaligned grains of case C are coupled by exchange and magnetostatic interactions. The angle θ between the easy axes of neighboring grains denotes the degree of alignment. The external field points antiparallel to one easy axis. For the calculations the material parameters of the $\text{Nd}_2\text{Fe}_{14}\text{B}$ phase ($A=7.7\times 10^{-12}\ \text{J/m}$, $J_s=1.61\ \text{T}$, $K_1=4.3\times 10^6\ \text{J/m}^3$, $K_2=0.65\times 10^6\ \text{J/m}^3$) and SmCo_5 ($A=12.0\times 10^{-12}\ \text{J/m}$, $J_s=1.06\ \text{T}$, $K_1=17.1\times 10^6\ \text{J/m}^3$) at $T=300\ \text{K}$ were taken from Hock¹² and Kütterer, Hilzinger, and Kronmüller,¹³ respectively.

The finite-element calculations provide the demagnetizing field at each point of the magnetic particles. As

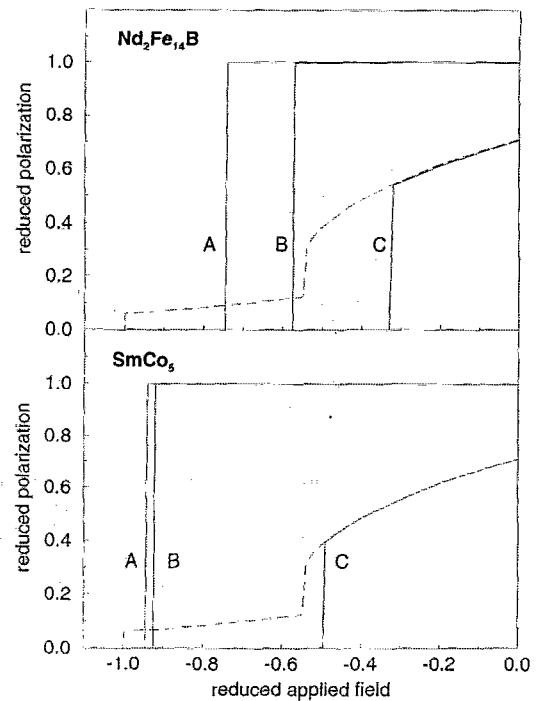


FIG. 2. The demagnetization curves of the samples show the effect of intergrain interactions in $\text{Nd}_2\text{Fe}_{14}\text{B}$ and SmCo_5 magnets. The spontaneous magnetic polarization normalized by its saturation value is plotted as a function of reduced magnetic field $h_{\text{ext}}/(2K_1/J_s)$. A: isolated grain; B: ideally oriented grains; C: interacting grains misaligned by 65° ; and the dashed line shows noninteracting Stoner-Wohlfarth particles.

shown in Fig. 1, large demagnetizing fields were found at the corners and at the interface of the particles.

The demagnetization curves, given in Fig. 2, characterize the magnetic properties of the different configurations. The comparison of the numerically calculated demagnetization curves reveals the effects that cause a reduction of the coercive field. The dashed curve represents the demagnetization curve of two noninteracting misori-

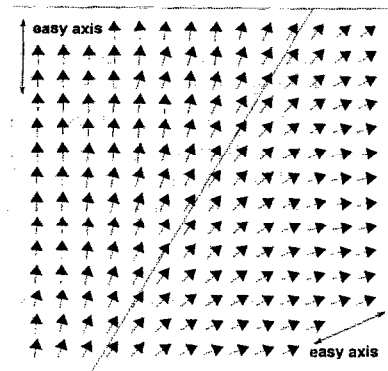


FIG. 3. Formation of an inhomogeneous magnetic state near the interface of misoriented particles owing to intergrain exchange and magnetostatic interactions. The plots show the spin arrangements for zero field in the vicinity of the grain boundary. The edge length of the enlarged area is $25\ \text{nm}$.

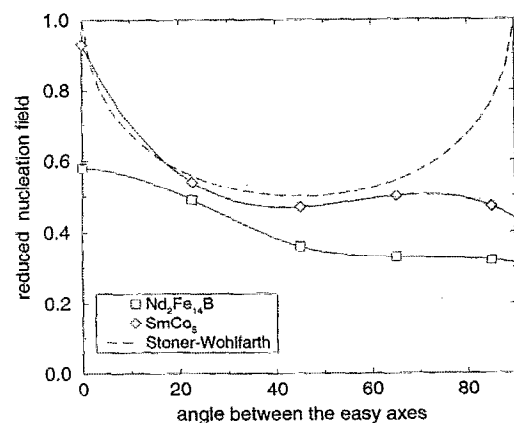


FIG. 4. The influence of misalignment on intergrain interactions in $\text{Nd}_2\text{Fe}_{14}\text{B}$ and SmCo_5 magnets. The nucleation field of magnetically coupled grains normalized by the ideal nucleation field $H_N^{\text{ideal}} = 2K_1/J_s$ is plotted as a function of the angle θ between the easy axes of the neighboring grains. The dashed curve represents the theoretical nucleation field for an ellipsoidal particle misoriented by the angle θ .

ented grains, obtained with conventional Stoner-Wohlfarth theory.

(i) The numerically calculated demagnetization curves for the isolated grains (A) have rectangular shape as obtained for ellipsoidal particles. However, in $\text{Nd}_2\text{Fe}_{14}\text{B}$ magnets the demagnetizing field reduces the coercive field considerably with respect to the ideal nucleation field of $H_N^{\text{ideal}} = 2K_1/J_s$.

(ii) A similar behavior holds for the ideally oriented particles (B). The long-range magnetostatic interactions between the grains cause a further reduction of the coercive field with respect to the coercivity of an isolated grain. Strong demagnetizing fields initiate magnetization reversal at the interface of the particles. Owing to the remarkably smaller value of the spontaneous magnetic polarization, the effect of internal stray fields is less significant in SmCo_5 than in $\text{Nd}_2\text{Fe}_{14}\text{B}$ magnets.

(iii) The demagnetization curve obtained for two non-interacting Stoner-Wohlfarth particles shows a step at the nucleation field of the misaligned grain. This step vanishes if the misaligned grains are magnetically coupled (C). The entire sample becomes demagnetized at an external field that is considerably smaller than the nucleation field of the misaligned grain. Intergrain exchange coupling provides an additional reduction of the nucleation field. The following section describes the results obtained for configuration C in more detail.

IV. NUCLEATION AT GRAIN BOUNDARIES OF MISALIGNED GRAINS

If misoriented grains are not separated by a nonmagnetic layer phase, the torque provided by the exchange

interaction and the demagnetizing field force the spontaneous magnetic polarization to rotate out of its easy axes near the interface of the particles. The magnetization pattern of Fig. 3 shows the strongly inhomogeneous magnetic state at the boundary within the two neighboring grains. In the very same region magnetization reversal is initiated. If the strongly inhomogeneous magnetic state becomes unstable, the spontaneous magnetic polarization reverses its orientation in the entire sample. Figure 4 shows the nucleation field of two misaligned grains coupled by magnetostatic and exchange interactions as a function of the angle θ between the easy axes. In contrast to conventional Stoner-Wohlfarth theory, the nucleation field of magnetically coupled grains does not show a significant increase for large misalignment ($45^\circ \leq \theta \leq 90^\circ$).

V. CONCLUSION

Numerical micromagnetic calculations show that interparticle interaction drastically affects the coercive field of nucleation controlled permanent magnets:

The long-range magnetostatic interactions between the grains considerably reduces the coercive field of ideally oriented particles with respect to the coercivity of an isolated grain; the exchange coupling of misaligned grains causes a further reduction of the coercive field, and low values of coercive field ($\approx 30\% - 40\%$ of the ideal nucleation field $H_N^{\text{ideal}} = 2K_1/J_s$) are found if the angle between the easy axes of adjacent grains is high; the numerical simulation of the magnetization reversal process in $\text{Nd}_2\text{Fe}_{14}\text{B}$ and SmCo_5 magnets confirms the nucleation of reversed domains at the interface of neighboring grains coupled by magnetostatic and exchange interactions.

¹W. F. Brown, Rev. Mod. Phys. **17**, 15 (1945).

²E. C. Stoner and E. P. Wohlfarth, Philos. Trans. R. Soc. **240**, 599 (1948).

³H. Kronmüller, J. Mag. Soc. Jpn. **15**, 6 (1991).

⁴A. Sakuma, S. Tanikawa, and M. Tokunaga, J. Magn. Magn. Mater. **84**, 52 (1990).

⁵H. Fukunaga and T. Fukuda, Jpn. J. Appl. Phys. **29**, 1711 (1990).

⁶H. Fukunaga and H. Inoue, Jpn. J. Appl. Phys. **31**, 1347 (1992).

⁷A. Hernando, I. Navarro, and J. M. González, Europhys. Lett. **20**, 175 (1992).

⁸H. F. Schmidts and H. Kronmüller, J. Magn. Magn. Mater. **94**, 220 (1992).

⁹Y. D. Yan and E. Della Torre, IEEE Trans. Magn. **MAG-24**, 2368 (1988).

¹⁰P. Fernandes, P. Girdinio, P. Molino, G. Molinari, and M. Repetto, IEEE Trans. Magn. **MAG-26**, 795 (1990).

¹¹T. Schrefl, H. F. Schmidts, J. Fidler, and H. Kronmüller, J. Magn. Magn. Mater.

¹²S. Hock, Ph.D. thesis, University of Stuttgart, Germany, 1988.

¹³R. Kütterer, H.-R. Hilzinger, and H. Kronmüller, J. Magn. Magn. Mater. **4**, 1 (1977).